The Princeton Open Ventilation Monitor Collaboration[1]
Princeton University,
Princeton, NJ 08544

Philippe Bourrianne
Department of Mechanical and
Aerospace Engineering,
Princeton University,
Princeton, NJ 08544

Stanley Chidzik
Department of Physics,
Princeton University,
Princeton, NJ 08544

Daniel J. Cohen
Department of Mechanical and
Aerospace Engineering,
Princeton University,
Princeton, NJ 08544

Peter Elmer
Department of Physics,
Princeton University,
Princeton, NJ 08544

Thomas Hallowell
Department of Anesthesiology and
Critical Care Medicine,
Children's Hospital of Philadelphia,
Philadelphia, PA 19104

Todd J. Kilbaugh
Department of Anesthesiology and
Critical Care Medicine,
Children's Hospital of Philadelphia,
Philadelphia, PA 19104

David Lange
Department of Physics,
Princeton University,
Princeton, NJ 08544

Andrew M. Leifer[2]
Princeton Neuroscience Institute and
Department of Physics,
Princeton University,
Princeton, NJ 08544
e-mail: leifer@princeton.edu

Daniel R. Marlow
Department of Physics,
Princeton University,
Princeton, NJ 08544

Peter D. Meyers
Department of Physics,
Princeton University,
Princeton, NJ 08544

Inexpensive Multipatient Respiratory Monitoring System for Helmet Ventilation During COVID-19 Pandemic

Helmet continuous positive applied pressure is a form of noninvasive ventilation (NIV) that has been used to provide respiratory support to COVID-19 patients. Helmet NIV is low-cost, readily available, provides viral filters between the patient and clinician, and may reduce the need for invasive ventilation. Its widespread adoption has been limited, however, by the lack of a respiratory monitoring system needed to address known safety vulnerabilities and to monitor patients. To address these safety and clinical needs, we developed an inexpensive respiratory monitoring system based on readily available components suitable for local manufacture. Open-source design and manufacturing documents are provided. The monitoring system comprises flow, pressure, and CO_2 sensors on the expiratory path of the helmet circuit and a central remote station to monitor up to 20 patients. The system is validated in bench tests, in human-subject tests on healthy volunteers, and in experiments that compare respiratory features obtained at the expiratory path to simultaneous ground-truth measurements from proximal sensors. Measurements of flow and pressure at the expiratory path are shown to deviate at high flow rates, and the tidal volumes reported via the expiratory path are systematically underestimated. Helmet monitoring systems exhibit high-flow rate, nonlinear effects from flow and helmet dynamics. These deviations are found to be within a reasonable margin and should, in principle, allow for calibration, correction, and deployment of clinically accurate derived quantities. [DOI: 10.1115/1.4053386]

Keywords: COVID-19, noninvasive ventilation, CPAP, helmet, hood, respiratory profile monitor, remote monitoring, critical care, low-cost ventilator, emergency ventilator

---

Edna Normand
Princeton Neuroscience Institute and
Department of Molecular Biology,
Princeton University,
Princeton, NJ 08544;
Rutgers Robert Wood Johnson,
New Brunswick, NJ 08901

Janine Nunes
Department of Mechanical and
Aerospace Engineering,
Princeton University,
Princeton, NJ 08544

Myungchul Oh
Department of Physics,
Princeton University,
Princeton, NJ 08544

Lyman Page
Department of Physics,
Princeton University,
Princeton, NJ 08544

Talmo Periera
Princeton Neuroscience Institute,
Princeton University,
Princeton, NJ 08544

Jim Pivarski
Department of Physics,
Princeton University,
Princeton, NJ 08544

Henry Schreiner
Princeton Institute for Computational Science
and Engineering Princeton University,
Princeton, NJ 08544

Howard A. Stone
Department of Mechanical and
Aerospace Engineering,
Princeton University,
Princeton, NJ 08544

David W. Tank
Princeton Neuroscience Institute,
Princeton University,
Princeton, NJ 08544

Stephan Thiberge
Princeton Neuroscience Institute,
Princeton University,
Princeton, NJ 08544

Christopher Tully
Department of Physics,
Princeton University,
Princeton, NJ 08544

1 Introduction

Noninvasive ventilation systems, such as continuous positive application of pressure (CPAP) and high flow nasal canula, have emerged as important tools for treating coronavirus disease 2019 (COVID-19) patients who need respiratory support but not intubation [1,2]. Such noninvasive approaches conserve traditional ventilators and improve patient outcomes by reducing or eliminating the need for invasive ventilation [3]. Additionally, COVID-19 patients show surprisingly poor outcomes on invasive ventilation [4], making noninvasive ventilation (where applicable) uniquely valuable during the pandemic.

Helmet noninvasive ventilation (NIV) is a form of CPAP that uses a clear, polyvinyl chloride, bubble-like helmet, attached to a soft collar that seals around a patient's neck [5]. The helmet delivers an air–oxygen mixture to the patient at a higher than atmospheric pressure with a positive end expiratory pressure (PEEP) valve. The PEEP serves to keep the patient's airways open and the patient oxygenated, increases the functional residual capacity of the lung, recruiting collapsed alveoli and decreasing the left ventricular transmural pressure, and assists through other mechanisms in augmenting patient respiratory function [6]. Helmet NIV is appealing for pandemic use because it can be run directly from a constant flow of air–oxygen, which is readily available in hospitals [7]. Helmets can be purchased for less than 300 USD, are straightforward to manufacture, and have been available during the pandemic, despite supply chain disruptions for other ventilators [8,9]. Importantly, helmet NIV is an enclosed system that uses viral filters to protect clinicians and other patients from droplets or aerosolized SARS-CoV-2 viral particles shed by the patient [10]. Helmet NIV is permitted by the United States Food and Drug Administration for COVID-19 treatment [11].

Despite these advantages, lingering safety concerns have prevented wider adoption of the helmet in the United States. Steady airflow is required to clear the patient's expired CO_2 from accumulating in the helmet [12]. An unexpected drop of airflow caused by a disruption in gas supply or blockage in the circuit could lead to rebreathing of CO_2 and asphyxiation [13]. Therefore, one of the greatest concerns when using helmets is the lack of an effective monitoring and alarm system. Antisuffocation valves can help mitigate this risk, but ultimately a dedicated monitoring and alarm system is needed to employ helmet NIV safely [14]. Partly for this reason, helmets in the U.S. have been primarily restricted to the intensive care unit, where clinician-to-patient ratios are high enough to allow clinicians to observe patients around-the-clock.

We have addressed these safety risks and clinical needs by developing an inexpensive respiratory profile monitoring system, which we call the Princeton open ventilator monitor (POVM), that is based on readily available commercial components and is suitable for rapid fabrication during a pandemic. The system is designed for use in conjunction with noninvasive helmet ventilator systems, such as the Sea-Long Medical Systems COVID-19 Helmet [8] and the Subsalve oxygen treatment hood [9], but is modular and can be used in other systems. The system comprises one or more flow, pressure, and CO_2 sensors per helmet, and includes a central station that can be used to remotely monitor up to 20 patients simultaneously. The system reports flow, pressure, and CO_2 concentration in the helmet, the patient's equivalent tidal volume ($\approx$TV), respiratory rate (RR), ratio of inspiratory to expiratory time (I:E ratio), peak inspiratory pressure (PIP), and PEEP. The system allows helmets to be deployed more broadly on the ward, since a single clinician can now monitor many patients simultaneously. The respiratory profile provided by the system allows clinicians to track disease progression and informs treatment decisions, including decisions about when to intubate.

We have produced and tested 50 such devices in an academic setting in a matter of weeks at a marginal cost of under 300 USD with volunteer labor. Commercial monitoring devices designed for mechanical ventilation, like the Philips Respirionics NM3 monitor, offer some of the functionality of our monitoring system, but those systems are currently unavailable due in part to disruptions in the medical supply chain. Moreover, commercial alternatives are all single-patient devices, are not designed for helmet NIV, and are expensive to purchase, making them poorly suited for rapid scale-up and deployment in a pandemic setting. For example, the cost to purchase commercial alternatives was 20–40 times more than the cost we incurred to produce our device with volunteer labor. The unique advantages of the device as well as the affordability of its parts suggest that it may be an attractive option for hospitals or others to self-manufacture in the context of a pandemic. To facilitate self-manufacture, we provide detailed parts lists, computer-aided design files, software, and instructions

for assembly and testing. The device has not undergone evaluation by any regulatory body and is not approved by the United States Food and Drug Administration.

2 Materials and Methods

2.1 Design and Construction of the Device and Software.
The Princeton Open Ventilation Monitor device consists of a flow-sensor assembly and an interface box located at the patient's bedside, as well as a multipatient remote monitoring station, as shown in Fig. 1. When used with a helmet for monitoring patients undergoing noninvasive ventilation, the flow-sensor assembly is inserted into the expiratory path. A schematic of the system is shown in Fig. 2. Detailed information can be found in Supplemental Material on the ASME Digital Collection (Supplementary Design and Construction of the Device and Software).

2.2 Methods for Testing and Evaluation of the Device and Software.

2.2.1 Software Testing. Software was designed with the following testing strategies in place: Static type analysis is performed to ensure basic validity of the code on every commit. Some portions of the code, such as the custom rolling window, have unit tests. A simulation and a data recording playback feature provide tools to perform integration tests for the hardware,
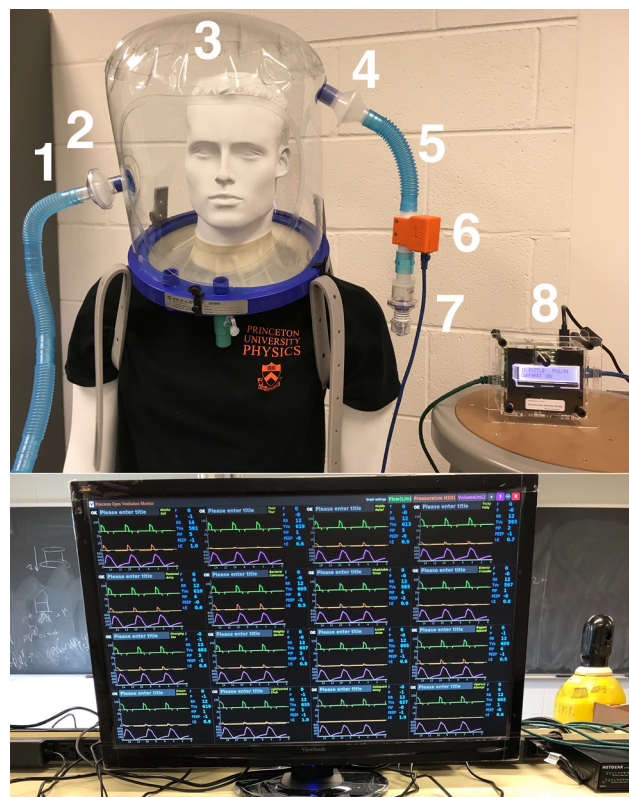

Fig. 1 Device monitors respiratory features by measuring pressure and flow of air leaving a helmet. Top: Device is shown installed in a typical circuit. Optional CO_2 sensor is not shown. (1) Inspiratory path. (2) Filter. (3) Patient in helmet. (4) Filter. (5) Expiratory path. (6) Flow-sensor assembly. (7) PEEP valve. (8) Interface box. The interface box reports basic respiratory information and announces audible and visual alarms if flow, pressure, or respiratory rate cross clinician defined thresholds. Bottom: The remote monitoring station displays flow, pressure, and volume waveforms and clinically relevant quantities including equivalent tidal volume, respiratory rate, I:E ratio, PIP and PEEP from up to 20 devices. Here, 16 devices in a test-circuit are being monitored simultaneously.
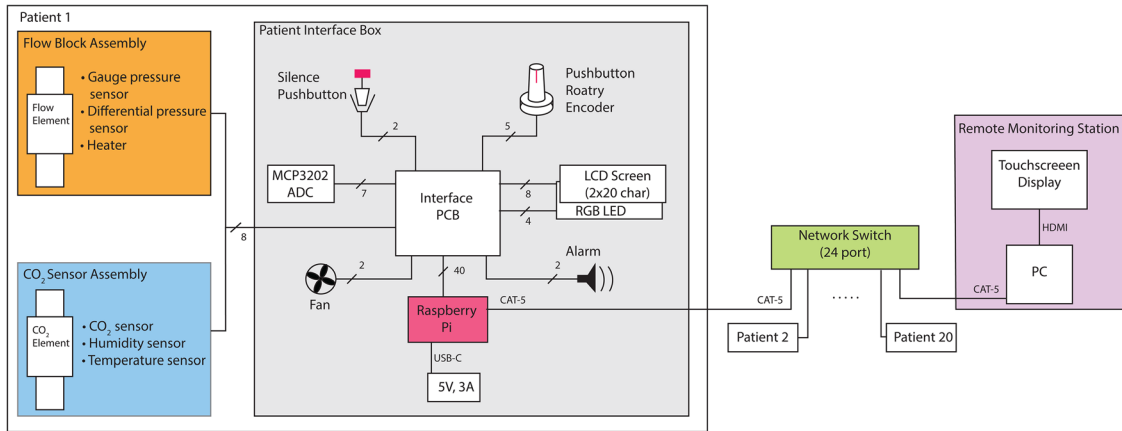
Fig. 2 Schematic of system design

analysis, and the clinician graphical user interface. An alternative patient loop that runs using Qt instead of requiring the hardware rotary, screen, and silence button enables testing with the playback even without a physical device present.

2.2.2 Flow-Sensor Assembly Calibration Tests. The flow-sensor assembly was calibrated by using a mass flow controller (Alicat Scientific MCR-100SLPM-D). As sketched in Fig. 3(*c*), the inlet port of the mass flow controller (MFC) was connected to compressed air and the outlet port was connected to the flow element by a long segment (1.5 m) of medical tubing. To minimize the effect of tubing curvature in the flow calibration (see tests below), the tubing upstream of the flow element was maintained

horizontal and straight, and downstream the flow element is directly connected to atmospheric pressure. Successive steps of constant flow Q ranging from 10 L/min to 100 L/min were imposed while the differential pressure ΔP at the flow sensor was measured using our device (see Fig. 3). The details of the sweep were chosen to probe both the steady-state relation between Q and ΔP and temporal dynamics during changes of applied flow. The 0–100 L/min flow range accessible to our MFC is clinically relevant to the helmet NIV application and corresponds to differential pressure ΔP readings from 0 to 150 Pa (Fig. 3(*b*)). The relation between ΔP (Fig. 3(*b*)) and Q (Fig. 3(*a*)), averaged over many flow elements, gives the calibration in Fig. 4 right. Flow elements with obvious manufacturing defects had Q-ΔP relations that
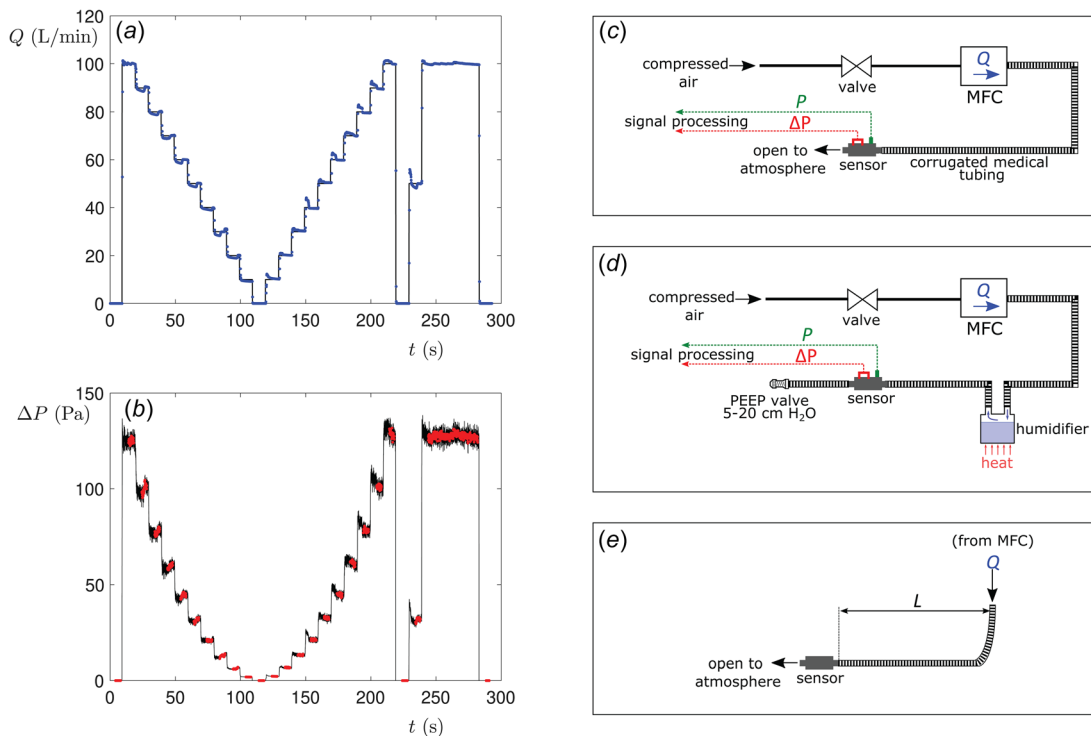

Fig. 3 Calibration of the flow sensor. (*a*) Standard flow sweep used to calibrate the flow sensor. Successive steps of flow Q (L/min) were imposed—the shaded points are the flow measured in the MFC. (*b*) The differential pressure ΔP (Pa) as measured by our flow sensor. Black points are raw data measured by the sensor at 50 Hz. Shaded points are derived from the black points by eliminating the beginning and end of each step and averaging to match the 10 Hz of data from the MFC. (*c*) Sketch of the standard configuration of our calibration setup. The MFC delivers a controlled flow Q to our flow element. (*d*) More tests were performed by adding a humidifier and a PEEP valve. (*e*) The influence of the tubing curvature was systematically tested by forcing a 90 deg bend at a distance L of the flow block.
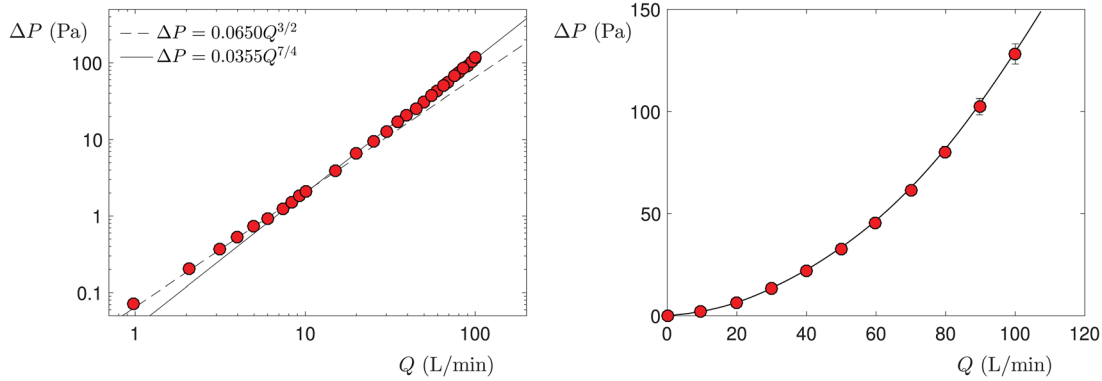
Fig. 4 Calibration curve for measuring flow from differential pressure. Left: Measurements of ΔP as function of the imposed flow Q for a single flow element. For low flow (below 15 L/min), $\Delta P \propto Q^{3/2}$ whereas $\Delta P \propto Q^{7/4}$ for larger flows. Right: Averaged measurements of ΔP as a function of the flow Q on 42 flow blocks machined by commercial firm Xometry. The error bars represent standard deviations. The solid line shows the lookup table that is installed in all of our devices.

deviated (see Fig. S3 available in the Supplemental Materials on the ASME Digital Collection), and were removed from the global calibration.

Similar calibrations were carried out in high relative humidity environment ($RH = 100\%$) for several hours (Fig. 3(d)) to verify the resilience of the sensor to humid air and possible condensation. The effect of the presence of a PEEP valve was also tested. The effect of the curvature of the tubing was systematically estimated by running calibration tests while forcing a 90 deg bend at a distance L of the input of the flow element (Fig. 3(e)).

2.2.3 Relationship Between Differential Pressure and Flow. Our device calculates the reported flow Q from a differential pressure measure ΔP across a portion of the flow element. A single global lookup table is used for all devices to convert from ΔP to Q (see Fig. 4). The relationship between Q and ΔP matches existing knowledge from fluid dynamics.

The geometry of the flow element and the Reynolds number determine this relation. The Darcy–Weisbach equation relates flow (here described as a flow velocity V) to differential pressure ΔP

$$\frac{\Delta P}{\frac{1}{2}\rho V^2 L/D} = f_D \tag{1}$$

given the length L and diameter D of a pipe, and a Darcy friction factor f_D that depends on the Reynolds number. At 100 L/min our device operates at an intermediate Reynolds number of $\text{Re} \approx 1800$, which is neither in the high ($\text{Re} \gg 2000$) nor low ($\text{Re} \ll 2000$) turbulence limits. ($\text{Re} = VD/\nu$, where the kinematic viscosity of air $\nu \simeq 2 \times 10^5 \text{ m}^2/\text{s}$. At $Q = 100$ L/min, air through one of the 19 honeycomb channels of diameter $D \simeq 3$ mm travels at approximately $V_1 \simeq 12$ m/s.)

The relation between a Darcy friction factor f_D and Reynolds number can be looked up in standard Moody diagrams [15]. For turbulent flow in sufficiently long smooth tubes, $f \propto \text{Re}^{-1/4}$, which implies $\Delta P \propto Q^{7/4}$. When our flow is lower, the Reynolds number drops. At a flow of 10 L/min ($\text{Re} = O(200)$), the flow in a shorter tube will have a growing boundary layer. In such laminar flow cases, we expect $\Delta P \propto Q^{3/2}$. We note that our calibration lookup table follows the $\Delta P \propto Q^{7/4}$ for high flows and the $\Delta P \propto Q^{3/2}$ for lower flows in agreement with expectations (Fig. 4).

2.2.4 Gage Pressure Test. The gage pressure sensor was calibrated by imposing a constant pressure with a pressure controller (Fluigent MFCS-EZ). The sensor saturates at a value around 3000 Pa and exhibits a linear response, see Fig. 5.

2.2.5 Methods for Bench Test Comparison to Commercial Medical Systems. To compare our device against commercial systems, we tested a prototype of our device on a commercial test

lung (IngMar ASL5000, IngMar Medical, Pittsburgh, PA) driven by a commercial ventilator (GE Avance CS2 Anesthesia System, GE Healthcare, Chicago, IL) in series with a commercial respiratory monitoring system (Philips Respironics NM3, Philips, Amsterdam, The Netherlands). Our device and the commercial test monitoring system were both situated in-line on the inspiratory path of the ventilator circuit. Simultaneous recordings of pressure and flow were made from our device, the commercial monitor, and the test lung system. Ground-truth volume information was also recorded from the test lung and precisely time-aligned. Pressure information from our device was also compared to the commercial monitor (NM3). Respiratory rate, PIP, and PEEP were also recorded from our device and occasionally compared to the display of the commercial ventilator. Our device was tested under a variety of ventilation modes including pressure control ventilation, volume control ventilation, and synchronized intermittent-mandatory ventilation with pressure control. The test lung's compliance was varied from 80 mL/cm-H_2O, typical for a healthy adult, to 20 mL/cm-H_2O, which is more typical of a diseased lung. Respiratory rate was set on either the ventilator or the lung to be approximately 15 breaths per minute.

2.2.6 Quality Control and Acceptance Testing of Final Assembled Devices. We developed a quality control protocol that could be used to test finished assembled devices prior to delivering to patients. The test demonstrates that each flow-sensor assembly's combination of specific flow element and sensors gives measured results for flow and pressure within a set range, for example, $\pm 10\%$ of actual values. This was done by providing a
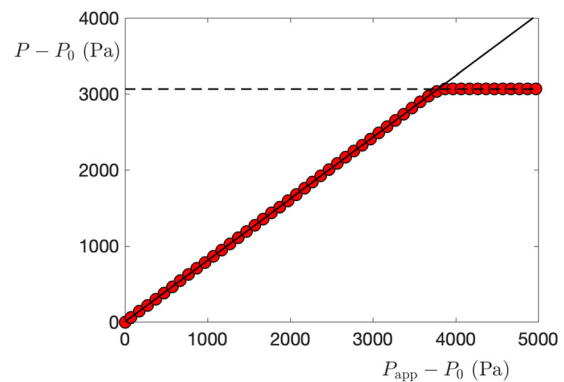

Fig. 5 Pressure sensor calibration. The pressure P measured varies linearly (solid line of slope 0.81) with the pressure P_{app} applied with the Fluigent pressure controller and saturates above 3000 Pa.
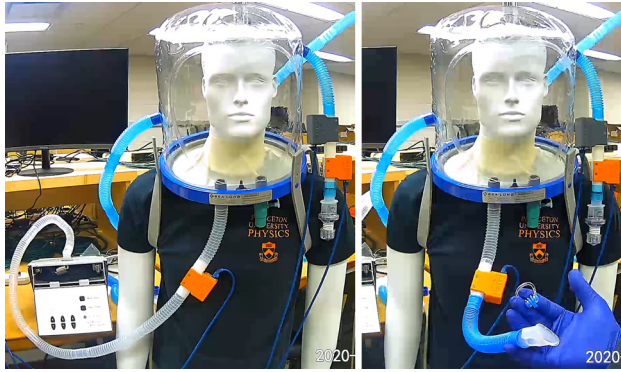
Fig. 6 Proximal sensor configuration. The auxiliary port of the helmet is used for external breathing, shown on the left with a mechanical breather and on the right with a spirometer mouthpiece. The expiratory path is instrumented with a CO_2 sensor in gray followed by a flow sensor in orange followed by a PEEP valve. The proximal flow sensor is placed directly inline between the spirometer mouthpiece and the auxiliary port.

known flow (using an Aalborg GFC47 mass flow controller, Aalborg Instruments & Controls, Orangeburg, NY) or known pressure (measured at a low flow using a water manometer sampling the flow just upstream of the flow element), recording sensor data with an interface box, analyzing the data using the fixed average calibrations discussed in Secs. 2.2.3 and 2.2.4, and comparing the recorded data to the known values.

2.3 Methods for Human Subject Test. Human subject tests were conducted in accordance with protocol # 12857 approved by Princeton University's Institutional Review Board. Written consent was obtained from a healthy adult volunteer. The subject was placed in a helmet (Sea Long Model PN5404, Sea-Long Medical Systems, Louisville, KY) fed by 80 L/min of medical air (AirGas) configured as shown in Fig. 1 with the PEEP valve set to its lowest limit, nominally 5 cm-H_2O. A one way valve (Teleflex model 1644) was added to one of the helmet ports to serve as an antisuffocation valve. The subject was in a standing position. The subject's spontaneous breathing was recorded on our respiratory monitor device over two 20 min trials as the subject was instructed to breath normally. A water manometer in our air delivery system appeared to contribute to dynamic changes to the volume in the helmet circuit coincident with the subject's breathing, so the manometer was inactivated during portions of the recording.

2.3.1 Proximal Sensor Configuration. A special setup was configured to make direct comparisons of proximal sensor readings to those measured in the expiratory path of the helmet. In these experiments, the human plugged their nose and breathed through a hose into the helmet, while the subject themselves remained outside the helmet. The auxiliary port of the helmet was used for external breathing, as shown in Fig. 6. The human subject breathed though a short 10-cm-long 22-mm-diameter tube with an inline flow and pressure sensor monitor, the proximal sensor. A spirometer mouthpiece and nose clip were used by the human subject.

Some bench tests were also performed in this configuration. In those instances, a mechanical breather instead of a human subject was connected through the inline flow sensor to the auxiliary port.

3 Results

3.1 Flow, Pressure, and Tidal Volume Agree With Commercial Test Systems During Mechanical Ventilation. To test our device's ability to measures of flow and pressure generally, we placed it in a circuit with a commercial single-patient respiratory monitoring system (Philips NM3) on a test lung (ASL-5000)

driven by a commercial mechanical ventilator. We compared recordings made by our device to those made by the test lung and the commercial monitoring system. Recordings from our device show strong agreement with the test lung for flow and volume, as shown in Figs. 7–9.

Our device's flow measurement showed closer agreement to the test lung than the commercial monitoring system that was measuring flow simultaneously. There was a scaling factor of about 5% discrepancy between our device and the test lung's measured flow, while the commercial monitor reported flows that differed from our device by a scaling factor of about 15% and an offset of 2 L/min. The commercial respiratory monitor also would occasionally show a flat line drift for flow or pressure during a breath, while our system captured dynamics of all breaths (see artifact at approximately 158 s in Fig. 7 and as a horizontal spread around zero in Fig. 9). This flat line (drift) from NM3 monitor is likely caused by the periodic flushing of the system to avoid condensation in the pressure lines.

In measures of pressure, our system had close agreement to the commercial respiratory monitor. We note that our system seemed to avoid quantization artifacts found in the commercial monitoring system at low pressures (see steps in pressure around 80 s in NM3 recording in Fig. 7).

We also compared derived quantities—the equivalent tidal volume, PIP, PEEP, and breathing rate—with those reported by the mechanical ventilator at the same time. Our system largely agrees with the ventilator's own settings (see Table 1).

3.2 Human Volunteer Helmet Noninvasive Ventilation Study. A healthy consenting adult volunteer was placed in a helmet and received medical air at 80 L/min while undergoing monitoring with our device. The device captures waveforms for flow, pressure, and equivalent tidal volume, as shown in Fig. 10. The measured respiratory rate matched that reported by the subject. Measured flow waveforms appear qualitatively similar to previous reports of human subjects in a helmet [12]. Recorded device data stream is available in Supplementary Data Files 1 available in the Supplemental Materials on the ASME Digital Collection.

3.2.1 Comparison of Tidal Volume Measured at Helmet Expiratory Path to That Measured Proximally. A central question in the applicability of helmet monitoring for clinicians is whether the patient's tidal volume and waveforms are modified by the pliable helmet. We had independently validated our device's volume estimates during mechanical ventilation with the ASL-5000 artificial lung (Fig. 8 where there was no helmet in the circuit). To quantify the effect of a helmet on our device's ability to estimate volume, we next conducted human-subject tests on volunteers wearing a helmet and directly compared simultaneous recordings at the expiratory path to measurements proximal to the patient. Here, the proximal sensor served as "truth" in the sense that it provides an ideal respiratory monitoring data with direct monitoring of flows, pressures, and computed tidal volumes from the human subject that should be unaffected by the helmet. The human stood outside of the helmet, plugged their nose, and breathed normally into the helmet through tubing connected to the helmet's auxiliary port. Readings were made simultaneously at the expiratory path. From the perspective of the expiratory path, the airflow behaves as if the patient were inside the helmet. The comparison of the proximal sensor (auxport) and expiratory pressures, flows, and estimated tidal volumes are shown in Fig. 11. Leaks were monitored through an inspiratory-to-expiratory path average flow rate comparison. Leaks were observed to be as large as 1–4 LPM, depending on the configuration and quality of the neck seal. Leaks impact the tidal volume baseline calculation and the dynamical response of the volume modulation of the helmet described in more detail below.

By comparing the proximal to expiratory path, several observations can be made that reveal effects of the helmet system on one's ability to measure respiratory features. The first is a
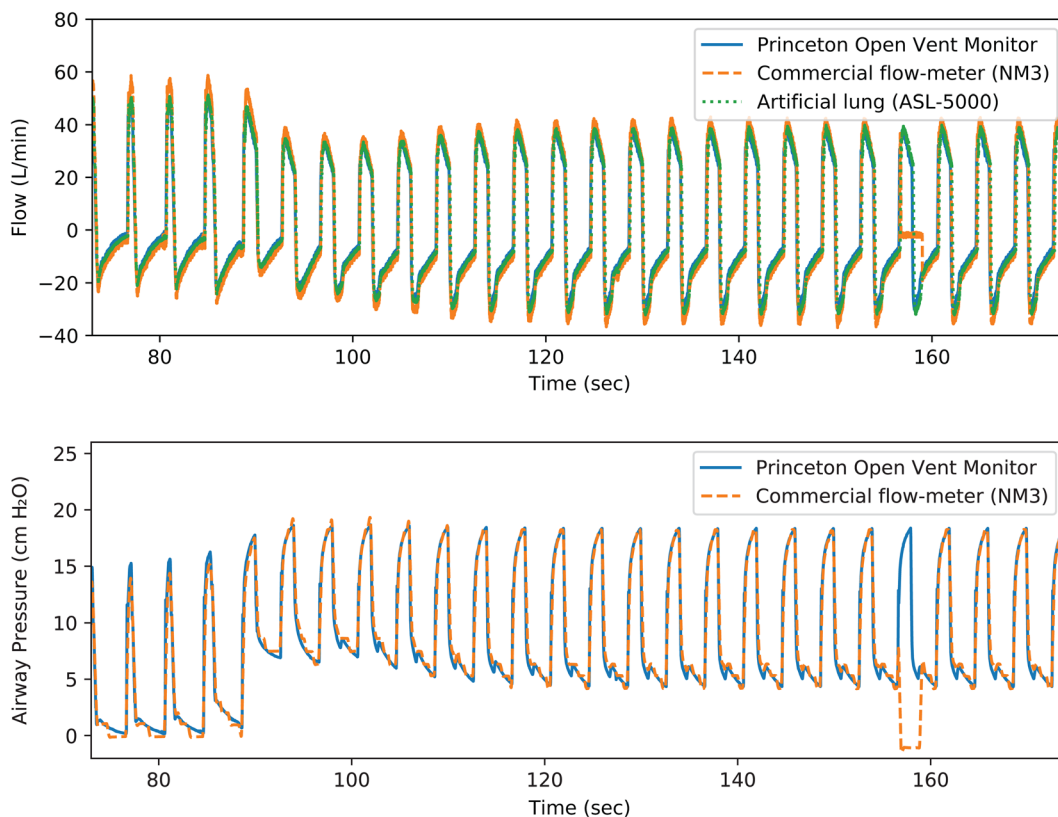
Fig. 7 Comparison to commercial monitor. Overlay of flow and pressure measured simultaneously from the Princeton open vent monitor, a commercial respiratory monitor (NM3), and an artificial lung (ASL-5000) driven by a commercial ventilator.
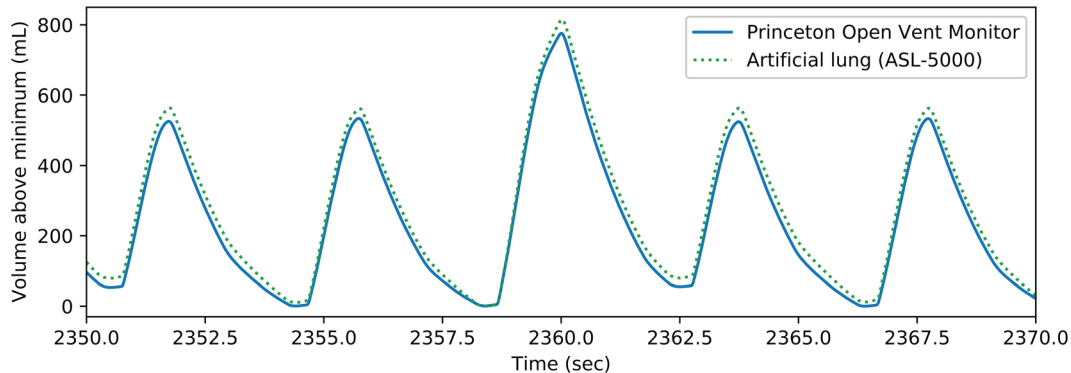

Fig. 8 Volume comparison to test lung. Overlay of derived volume from the Princeton Open Vent Monitor (using the high-pass filter with the weaker 0.0004 Hz Butterworth critical frequency) and measured volume from an artificial lung (ASL-5000), driven by a commercial ventilator.

discrepancy in pressure. In the top plot of Fig. 11, there is an additional pressure on the human subject side of the flow block of the proximal sensor of approximately 1 cm-H_2O. This pressure increase is attributed to the flow restriction inherent in the flow block and the short length of 22-mm tube to access the auxiliary port. The second is an expected change in baseline flow. From the middle plot of Fig. 11, the expiratory waveforms are offset from zero by the flushing rate of medical air through the helmet. In contrast, the average flow in and out of the proximal sensor is zero, as this is only connected to the human lung (nose clips are worn by the human subject).

Third is an observation that the expiratory waveforms appear to be slightly smoother than the proximal ones and in certain cases when a sharp feature appears in the proximal sensor, the expiratory path response is slower. To further explore the slow down of

response to the respiratory waveforms, a mechanical breather (QuickLung Breather from IngMar Medical, Pittsburgh, PA) was connected through the auxiliary port in the same configuration as the proximal sensor human subject test. The mechanical breather was configured to generate sharp respiratory waveforms (compliance, C, of 50 mL/cm-H_2O and a resistance, R_p, of 5 cm-H_2O/L/s). A comparison of the proximal sensor and expiratory sensor at an 80 L/min average flow rate through the Sea-Long helmet are shown in Fig. 12. The slow down in response as measured via the expiratory path is visible in the middle plot. Similar effects to those in Fig. 11 are observed in the pressure and estimated tidal volumes. Additional measurements were made at different settings of the mechanical breather, including resistance at 20 cm-H_2O/L/s and 50 cm-H_2O/L/s. At 50 cm-H_2O/L/s ($R_pC = 2 \cdot 5$ s), many of the sharp features in the mechanical breather waveforms
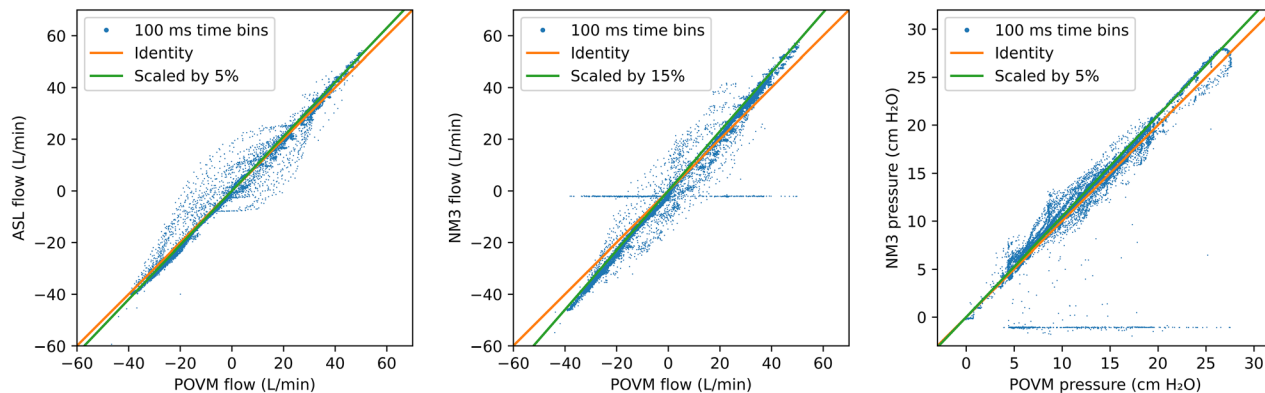
Fig. 9 Fine comparison of POVM, the artificial lung simulator (ASL), and a commercial respiratory monitor (NM3) in matched time-bins (100 ms wide). The commercial monitor occasionally drops to zero and has discretization effects at low pressure. POVM and ASL agree in flow up to a 5% scale factor; POVM and NM3 agree in flow up to a 15% scale factor, and POVM and NM3 agree in pressure up to a 5% scale factor.

Table 1 Comparison of derived quantities

	POVM derivation	Ventilator reading	NM3 reading
TV	440 mL	500 mL (setting)	460 mL
PIP	28.0 cm H_2O	29 cm-H_2O	
PEEP	4.5 cm-H_2O	5 cm-H_2O	
RR	15.0 bpm	15 bpm	
I:E	0.66		

POVM derived tidal volume equivalent ($\approx$ TV), PIP, PEEP, and breathing rate (RR) compared with contemporaneous readings/settings from the ventilator and readings from the commercial monitor (NM3).

are removed and the expiratory and proximal sensor waveforms agree. The apparently longer resistance-compliance time is an artifact of the helmet monitoring.

Finally, on the bottom plot of Fig. 11, the equivalent tidal volumes underestimate the expiratory path tidal volumes by roughly 20%. The accuracy of the equivalent tidal volume estimates from the expiratory path in the proximal sensor configuration was further evaluated with a calibrated 1-L volume syringe (Aspire 1 L volume calibration syringe) that was manually operated. The data from this comparison are shown in Fig. 13 for helmet flow rates of 50 L/min and 80 L/min. The underestimation of the equivalent tidal volumes is up to −20% at high flow rate.

The origin of this deviation is inherent and universal to the helmet continuous positive applied pressure setup and therefore of upmost important to clinicians that make use of these systems to infer tidal volume information about the patient. The physics origin of this deviation in tidal volume estimation is of similar origin to the slow down in response presented in Fig. 12. The pressure differential required to increase the flow rate through the expiratory path grows nonlinearly as $\Delta P \propto Q^{7/4}$ for large flows, as shown in Fig. 4. Therefore, a fraction of the exhaled volume at high flow rate will preferentially inflate the pliable helmet volume. Similarly, the inhaled volume will tend to contract a fraction of the helmet volume. Slight changes in the helmet volume (inflating and contracting) at high flow rate through the helmet are observed and can be exacerbated by deep, rapid, breathing of large tidal volumes.

It is therefore vital that helmet monitoring systems provide a tidal volume estimation that accounts for the inflation and deflation of the helmet volume and leaks, as the expiratory flow does not directly measure the volume change within the helmet. The bias toward underestimation of the equivalent tidal volumes at high flow rate can be removed with a correction factor that follows the same functional form of $\Delta P \propto Q^{7/4}$ for large flows. After

this flow rate-dependent correction, the deviations on tidal volumes are within ±5%. We have further added this correction as an option into the system so that a clinician can see the corrected value.

3.2.2 CO_2 in the Helmet. The CO_2 concentration in the helmet was monitored with the CO_2 sensor block at the expiratory path, Fig. 14. When Medical Air gas was flowed through the helmet at approximately 80 L/min without any human, the CO_2 concentration was measured to be 412±92 ppm, in agreement with expected CO_2 levels for fresh air.

CO_2 concentrations at the expiratory port were than measured when a human, standing external to the helmet, breathed into the helmet through the auxiliary port (Fig. 6). Measurements were made during three different flow rates, ranging from 50 L/min to over 100 L/min, Fig. 14 "auxiliary port breathing." The CO_2 concentration measured in the helmet as a function of flow rate reproduces previous findings [12].

CO_2 concentration was also measured at the expiratory port when the human test subject breathed from within the helmet ("helmet breathing" in Fig. 14, flow rate of approximately 93 L/min). At the nominal average flow rate of 80 L/min, the CO_2 concentration was measured to be approximately 3000 ppm. At 50 L/min, the average CO_2 concentration grows to 5000 ppm. The CO_2 concentration, measured every 2 s, fluctuates significantly. In the human subject test at an average flow rate of 93 L/min, the mean value of the CO_2 concentration was 3317 ppm and the root-mean-squared fluctuations of measurements were 732 ppm. Some of these fluctuations are due in part to the changes in flow rate that occur from subject breathing. But, even more so, we suspect the large fluctuations arise from incomplete mixing of the subject's exhaled CO_2 with the air in the helmet before it reaches the sensors in the expiratory path.

Fluctuations in measured CO_2 make it difficult to use CO_2 to reliably monitor fast time-varying changes to CO_2 dynamics. In contrast, flow and pressure can be monitored quickly, and they also correlate well with average CO_2 concentration.

3.3 External Sources of Variability. We tested the influence of relative humidity on our sensors, Fig. 3(*d*). In bench tests, we challenged our device by measuring 20 h of continuous flow of saturated humid air ($RH = 100\%$). Both sensors performed even in the presence of significant condensation in the flow element, which suggests that our heater circuit, designed to counter condensation, functions effectively. In tests with variable humidity, we observed that the flow Q increased slightly by less than 3% while the humidity rose from 5 to 100%.

Finally, the presence of curvature in tubing has been reported to affect measures of downstream flow [16,17]. This is relevant
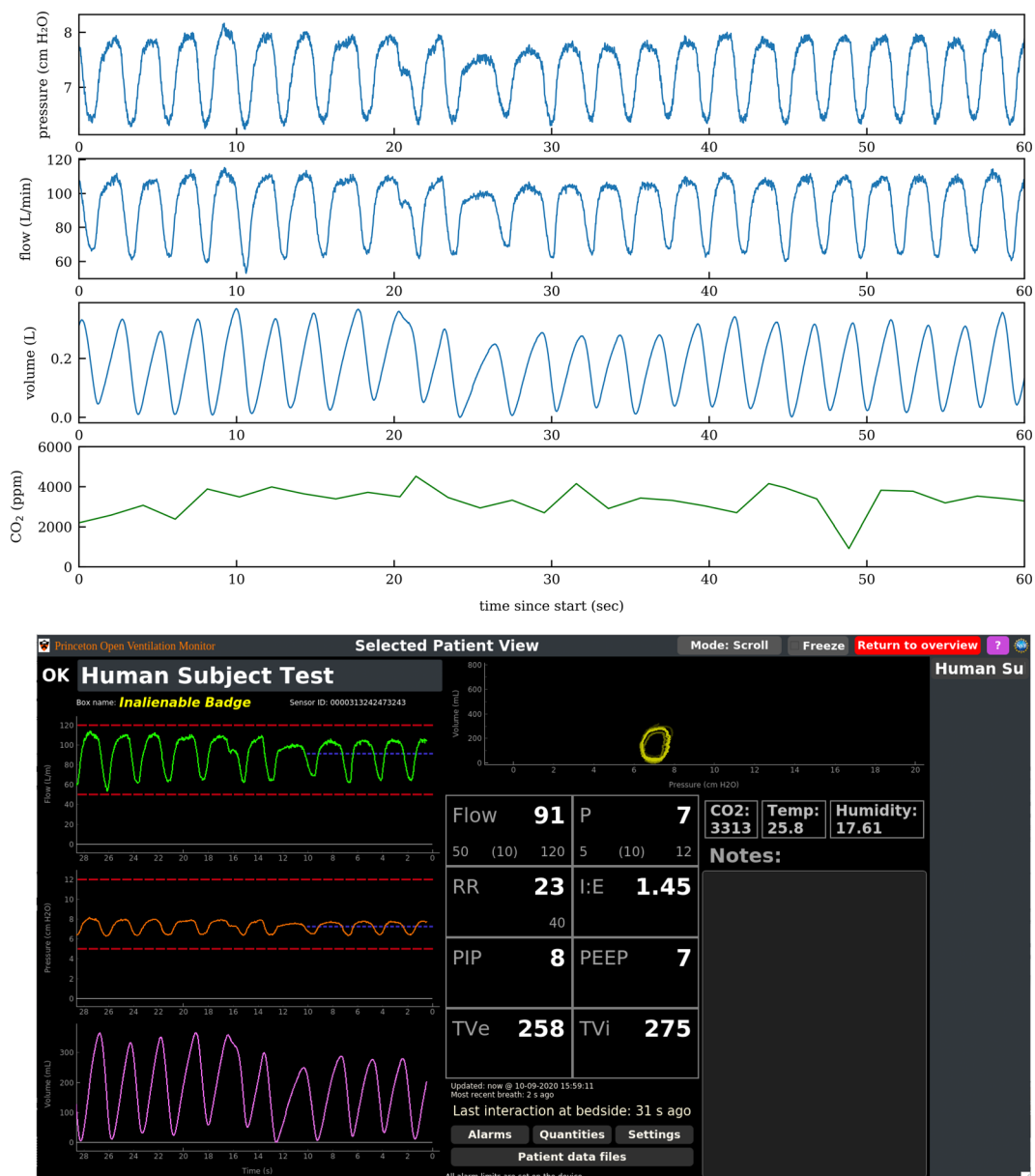
Fig. 10 Respiratory profile of healthy human subject in helmet. Top: Pressure, flow, equivalent tidal volume, and CO₂ concentration on the expiratory path of a helmet worn by a healthy human subject are shown. Positive flow is defined to be gas leaving the helmet through the expiratory path. Bottom: Derived quantities, including tidal volume, and respiratory rate, are visible on the remote monitoring station (shown here in "drilldown" screen).

because our device may dangle off the helmet at an angle, as can be seen in Figs. 1 and 6. We introduced a 90-deg bend into the tubing a variable distance L upstream of our device and observed the change in our device's reported flow Q under a constant imposed flow of 100 L/min, Figs. 3(e) and 15. We observed a systematic increase in the flow Q reported by our device for bends less than 30 cm upstream of our device. The largest deviations from the imposed flow occurred when the bend was closest to the device (5% for $L = 5$ cm).

3.4 Results of Production Run. We completed a production run of 50 devices. Producing devices at scale posed additional challenges regarding calibration and quality control. In particular manufacturing defects in the flow element altered the relationship between the measured pressure difference ΔP and the flow Q across the device, as shown in Fig. S3 available in the Supplemental Materials on the ASME Digital Collection. Initial

determination of ΔP versus Q for each flow element with a fixed sensor array allowed us to identify and remove defective devices, and eliminate outliers from the determination of the average calibration. After each flow element is integrated into its final flow-sensor assembly, it will undergo the acceptance testing described in Sec. 2.2.6. An example test result is shown in Fig. 16. A production yield of 88% was achieved on the flow-sensor assemblies after requiring the calibrations to stay within a 10% band of the nominal calibration above 15 L/min and above 5 cm-H_2O as a quality control measure.

To validate the multipatient functionality, we ran 40 devices on a test circuit continuously for six months to a year while simultaneously monitoring 20 devices each on two multipatient monitoring stations. Data cleanup was needed on the time scale of 2 weeks to 4 months depending on the multipatient disk storage, but otherwise the systems performed without obvious issues.
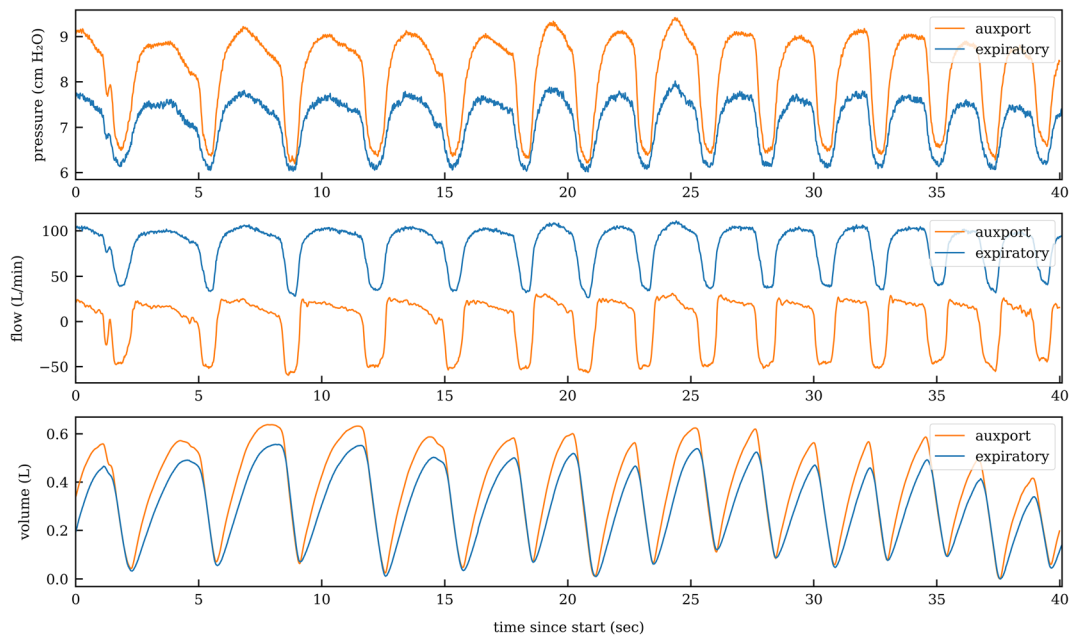
Fig. 11 Proximal versus expiratory sensor comparison, with human subject. The respiratory waveforms recorded directly by a proximal sensor (auxport) are compared to measurements made at the expiratory path. A slight pressure increase is seen by the human subject due to breathing through the proximal sensor and tube through the auxiliary port. Expiratory path's measure of flow appears slightly smoother compared to the proximal sensor, and the expiratory path measure of volume consistently underestimates that of the proximal sensor.
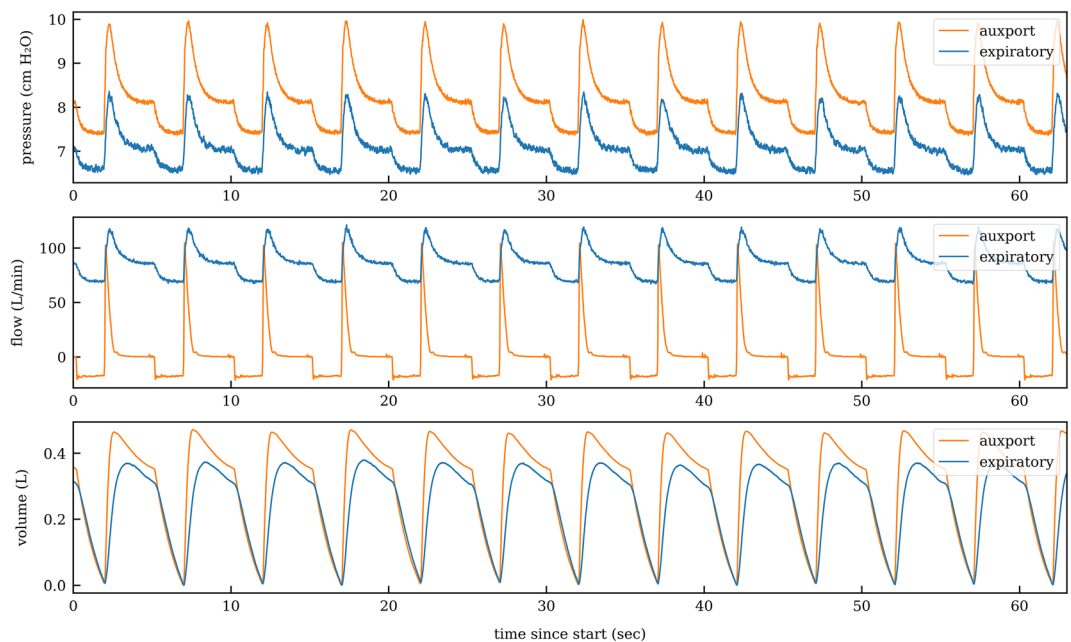
Fig. 12 Proximal versus expiratory sensor comparison, with mechanical breather. The IngMar medical QuickLung breather is connected in the proximal sensor configuration to the auxiliary port of the Seal-Long helmet and monitored simultaneously through the expiratory path of the helmet. The mechanical breather is set to a compliance of 50 mL/cm-H$_2$O and a resistance of 5 cm-H$_2$O/L/s to generate sharp respiratory waveforms at 12 bpm. The slow down in response as measured via the expiratory path is visible.

4 Discussion and Conclusions

We performed comparisons between our device and various references including test lungs, commercial monitors, calibrated syringes, and measurements made proximal to the subject, to assess our device's ability to accurately report clinically relevant respiratory features of a human in a helmet. Most of our measurements are in agreement but we do observe two types of disagreements related to flow and volume. The first is a 5–15% constant scaling discrepancy in flow rate (and correspondingly in volume), as observed in comparisons to either a calibrated test lung or commercial monitor, respectively, on an invasive ventilation test circuit. The other disagreement is a flow-dependent discrepancy between expiratory path measurements and proximal
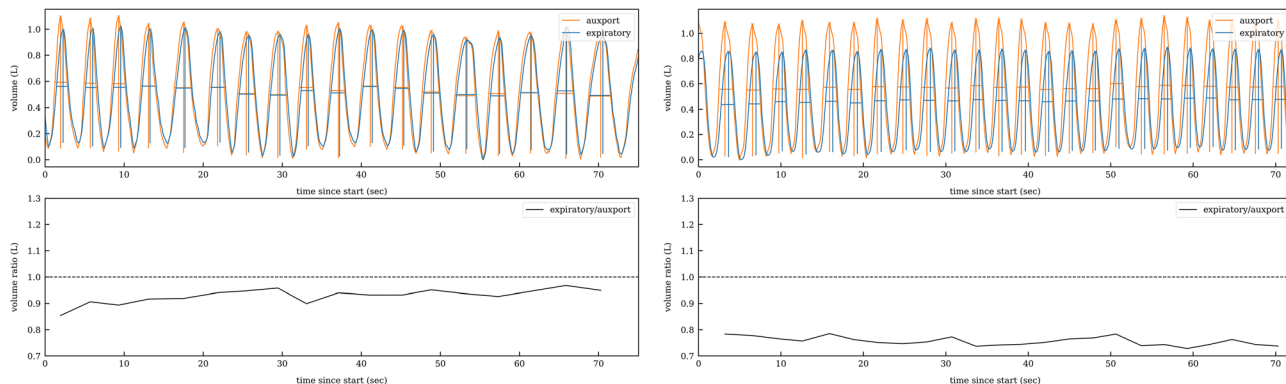
Fig. 13 Proximal versus expiratory sensor comparison, with 1 L calibrated syringe. The Aspire 1 L volume calibration syringe is operated manually in the proximal sensor configuration. The left plot is for a 50 L/min flow rate through the helmet and the right plot is for 80 L/min. The bottom plots are the corresponding ratios of the peak heights, where the peak heights are the equivalent tidal volume estimates. The underestimation of the equivalent tidal volumes by the expiratory sensor is up to 20% at high flow rate compared to the proximal sensor (auxport).
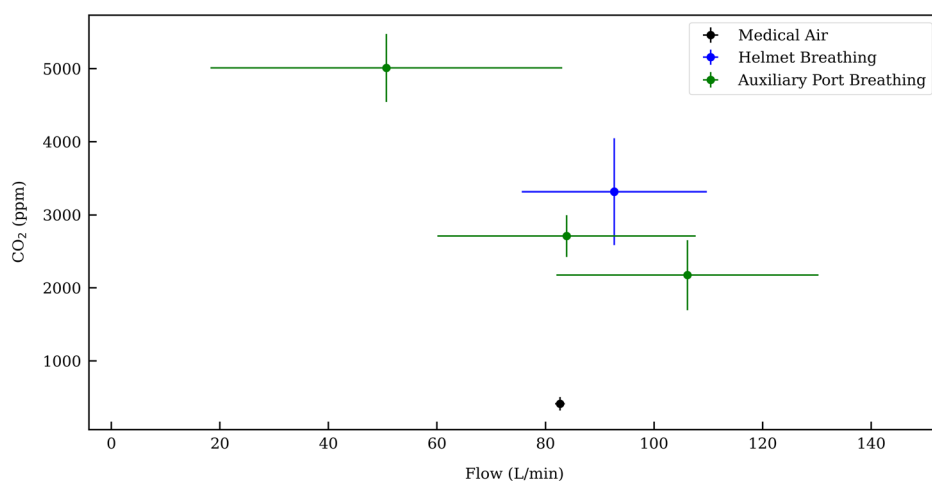
Fig. 14 CO_2 concentration in the helmet. The CO_2 concentration in the helmet as a function of flow rate reproduces previous findings [12]. The horizontal uncertainties are the RMS values of the flow measurements coming from the breathing of the human subject. The vertical uncertainties are the RMS values of the CO_2 concentration measurements in the expiratory path, indicating incomplete mixing of the exhaled breaths with the helmet flow. The steady-flow medical air measurement through the helmet shows that the intrinsic CO_2 concentration measurements are not a large contribution to the uncertainties compared to breathing.
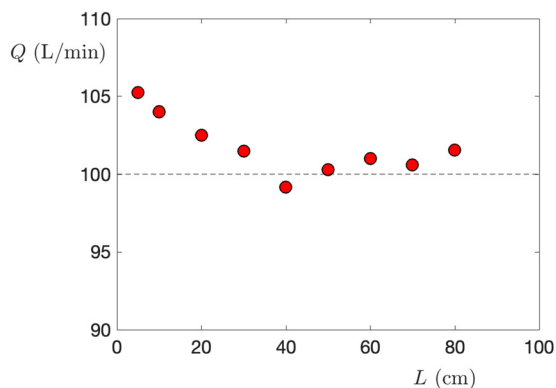
Fig. 15 Effect of bent tubing. Flow Q measured by our flow sensor in the presence of a 90 deg bend positioned a distance L upstream of the flow block. A 100 L/min flow was imposed by a Mass Flow Controller.

measurements. Of the two, we believe the latter is more clinically relevant as this impacts the clinician's ability to accurately distinguish flow and pressure dependent instrumentation effects from actual changes in the patient's tidal volume, which could be used to interpret a patient's progression in disease or recovery. To address this we proposed a software based calibration that brings this discrepancy to within 5%. The clinical impact of tidal volume estimation is particularly important to avoid ventilator-induced lung injury from an elevated pressure-support level [18–21].

The work here addresses two important gaps in the literature. We present what is, to our knowledge, the first report and characterization of a device designed explicitly to measure respiratory features of subjects undergoing helmet NIV. Recent clinical studies have emphasized that measuring tidal volumes accurately with helmet NIV is challenging and that patients undergoing helmet NIV who experienced treatment failure may have been exposed to injurious high tidal volumes during assisted spontaneous breathing [22,23].

We also fulfill another important gap in the area of rapid low-cost do-it-yourself emergency ventilators. While many emergency ventilator designs exist [24–27], none target noninvasive ventilation, and all lack detailed multipatient monitoring devices.
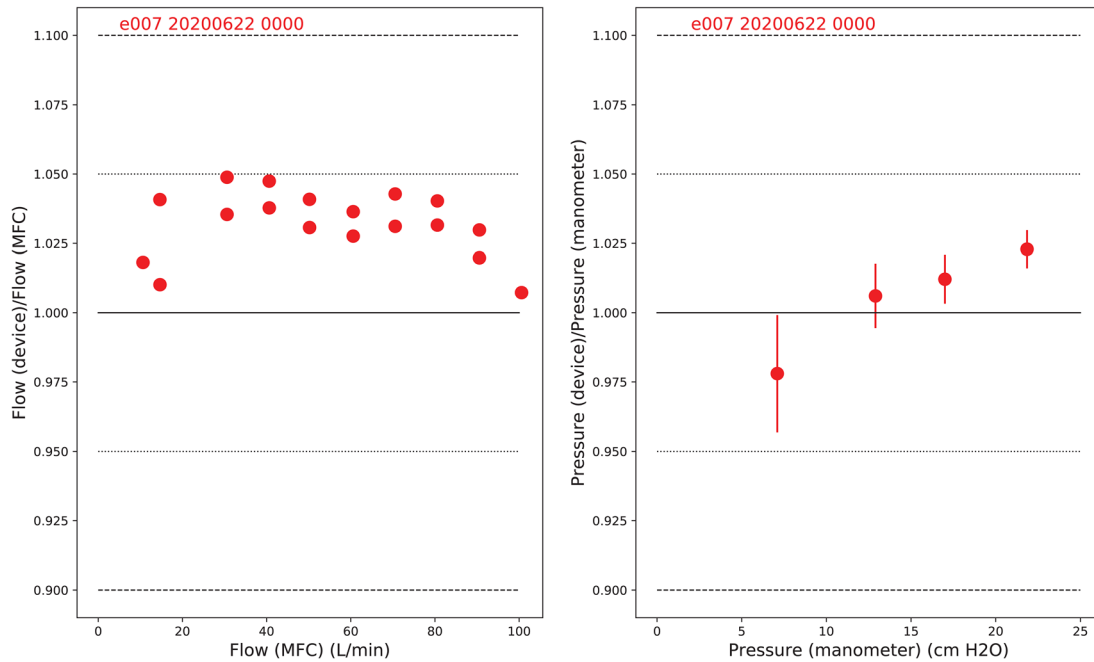
Fig. 16 Results of acceptance testing of a final flow-sensor assembly. Left: comparison of calibrated flow reported by the device under a test to flow set by a mass flow controller. Right: comparison of calibrated pressure reported by the device under test to pressure measured with a water manometer. Red text uniquely identifies the flow-sensor assembly.

Our device has the potential to improve patient outcomes and to mitigate well-documented safety concerns regarding CO_2 rebreathing that have prevented the helmet's widespread adoption. Our device also introduces the ability to monitor many patients simultaneously. Importantly, our device uses off-the-shelf components that have shown themselves to be robust to supply chain disruptions. The device is well suited for local manufacture during a pandemic.

References

[1] Grasselli, G., Pesenti, A., and Cecconi, M., 2020, "Critical Care Utilization for the COVID-19 Outbreak in Lombardy, Italy: Early Experience and Forecast During an Emergency Response," JAMA, **323**(16), p. 1545.

[2] Phua, J., Weng, L., Ling, L., Egi, M., Lim, C.-M., Divatia, J. V., and Shrestha, B. R., et al., 2020, "Intensive Care Management of Coronavirus Disease 2019 (COVID-19): Challenges and Recommendations," Lancet. Respir. Med., **8**(5), pp. 506–517.

[3] Patel, B. K., Wolfe, K. S., Pohlman, A. S., Hall, J. B., and Kress, J. P., 2016, "Effect of Noninvasive Ventilation Delivered by Helmet Vs Face Mask on the Rate of Endotracheal Intubation in Patients With Acute Respiratory Distress Syndrome: A Randomized Clinical Trial," JAMA, **315**(22), pp. 2435–2441.

[4] Richardson, S., Hirsch, J. S., Narasimhan, M., Crawford, J. M., McGinn, T., Davidson, K. W., and Barnaby, D. P., et al., 2020, "Presenting Characteristics, Comorbidities, and Outcomes Among 5700 Patients Hospitalized With COVID-19 in the New York City Area," JAMA, **323**(20), p. 2052.

[5] Antonelli, M., Conti, G., Pelosi, P., Gregoretti, C., Pennisi, M. A., Costa, R., Severgnini, P., Chiaranda, M., and Proietti, R., 2002, "New Treatment of Acute Hypoxemic Respiratory Failure: Noninvasive Pressure Support Ventilation Delivered by Helmet–a Pilot Controlled Trial," Crit. Care Med., **30**(3), pp. 602–608.

[6] Lepper, P. M., and Muellenbach, R. M., 2020, "Mechanical Ventilation in Early Covid-19 Ards," EClinicalMedicine, **28**, p. 100616.

[7] Savickaite, A., 2020, "Video: Non-Invasive CPAP by Helmet Setup COVID-19, Maurizio Franco Cereda, MD," Helmet Based Ventilation, Chicago, IL, accessed Apr. 20, 2020, https://www.helmetbasedventilation.com/post/video-non-invasive-cpap-by-helmet-setup-covid-19-maurizio-franco-cereda-md

[8] Sea-Long Medical Systems, 2020, "Sea-Long Medical Systems," Sea-Long Medical Systems, Louisville, KY, accessed May 5, 2020, http://www.sea-long.com/

[9] Lombardi Undersea LLC, 2020, "Lombardi Undersea LLC," Lombardi Undersea LLC, Middletown, RI, accessed Jan. 13, 2021, http://www.oxygentreatmenthoods.com/

[10] Cabrini, L., Landoni, G., and Zangrillo, A., 2020, "Minimise Nosocomial Spread of 2019-nCoV When Treating Acute Respiratory Failure," Lancet, **395**(10225), p. 685.

[11] U.S. Food and Drug Administration, 2020, "Enforcement Policy for Ventilators and Accessories and Other Respiratory Devices during the Coronavirus Disease 2019 (COVID-19) Public Health Emergency," U.S. Food and Drug Administration, Rockville, MD, accessed Jan. 13, 2021, https://www.fda.gov/regulatory-information/search-fda-guidance-documents/enforcement-policy-ventilators-and-accessories-and-other-respiratory-devices-during-coronavirus

[12] Taccone, P., Hess, D., Caironi, P., and Bigatello, L. M., 2004, "Continuous Positive Airway Pressure Delivered With a "Helmet": Effects on Carbon Dioxide Rebreathing," Crit. Care Med., **32**(10), pp. 2090–2096.

[13] Patroniti, N., Saini, M., Zanella, A., Isgrò, S., and Pesenti, A., 2007, "Danger of Helmet Continuous Positive Airway Pressure During Failure of Fresh Gas Source Supply," Intensive Care Med., **33**(1), pp. 153–157.

[14] Milan, M., Zanella, A., Isgrò, S., Deab, S. A. E. A. E. S., Magni, F., Pesenti, A., and Patroniti, N., 2011, "Performance of Different Continuous Positive Airway Pressure Helmets Equipped With Safety Valves During Failure of Fresh Gas Supply," Intensive Care Med., **37**(6), pp. 1031–1035.

[15] Moody, F., 1944, "Friction Factors for Pipe Flow," Trans. ASME, **66**, pp. 671–684.

[16] Dean, W., 1928, "LXXII. the Stream-Line Motion of Fluid in a Curved Pipe (Second Paper)," London, Edinburgh, Dublin Philos. Mag. J. Sci., **5**(30), pp. 673–695.

[17] Hellström, L. H. O., Zlatinov, M. B., Cao, G., and Smits, A. J., 2013, "Turbulent Pipe Flow Downstream of a 90° Bend," J. Fluid Mech., **735**, p. R7.

[18] Frat, J.-P., Thille, A. W., Mercat, A., Girault, C., Ragot, S., Perbet, S., and Prat, G., et al., 2015, "High-Flow Oxygen Through Nasal Cannula in Acute Hypoxemic Respiratory Failure," New Engl. J. Med., **372**(23), pp. 2185–2196.

[19] Dreyfuss, D., and Saumon, G., 1993, "Role of Tidal Volume, FRC, and End-Inspiratory Volume in the Development of Pulmonary Edema Following Mechanical Ventilation," Am. Rev. Respir. Dis., **148**(5), pp. 1194–1194.

[20] Slutsky, A. S., and Ranieri, V. M., 2013, "Ventilator-Induced Lung Injury," New Engl. J. Med., **369**(22), pp. 2126–2136.

[21] De Prost, N., Ricard, J.-D., Saumon, G., and Dreyfuss, D., 2011, "Ventilator-Induced Lung Injury: Historical Perspectives and Clinical Implications," Ann. Intensive Care, **1**(1), pp. 1–15.

[22] Munshi, L., and Hall, J. B., 2021, "Respiratory Support During the Covid-19 Pandemic: Is It Time to Consider Using a Helmet?," JAMA, **325**(17), pp. 1723–1725.

[23] Spinelli, E., Mauri, T., Beitler, J. R., Pesenti, A., and Brodie, D., 2020, "Respiratory Drive in the Acute Respiratory Distress Syndrome: Pathophysiology, Monitoring, and Therapeutic Interventions," Intensive Care Med., **46**(4), pp. 606–618.

[24] Abba, A., Accorsi, C., Agnes, P., Alessi, E., Amaudruz, P., Annovi, A., and Desages, F. A., et al., 2021, "The Novel Mechanical Ventilator Milano for the Covid-19 Pandemic," Phys. Fluids, **33**(3), p. 037122.

[25] Raymond, S. J., Wesolowski, T., Baker, S., Liu, Y., Edmunds, J. L., Bustamante, M. J., Ley, B., et al., 2020, "A Low-Cost, Rapidly Scalable, Emergency Use Ventilator for the Covid-19 Crisis," medRxiv, epub.

[26] Kwon, A. H., Slocum, A. H., Varelmann, D., Nabzdyk, C. G. S., Araki, B., Abu-Kalaf, M., and Detienne, M., et al., 2020, "Rapidly Scalable Mechanical Ventilator for the Covid-19 Pandemic," Intensive Care Med., **46**(8), pp. 1642–1644.

[27] LaChance, J., Zajdel, T. J., Schottdorf, M., Saunders, J., Dvali, S., Seirup, L., Marshall, C., Notterman, D. A., and Cohen, D. J., 2020, "PVP1–The People's Ventilator Project: A Fully Open, Low-Cost, Pressure-Controlled Ventilator," medRxiv, epub.